# The influence of elevated Fe and Zn impurities on the rapid solidification behaviour of AA6061 processed using single-track laser surface melting

Janelle Faul<sup>1</sup>, Mark A. Whitney<sup>1</sup>, Haiou Jin<sup>2</sup>, Mary A. Wells<sup>1</sup>, Michael J. Benoit<sup>1,\*</sup>

- <sup>1</sup> University of Waterloo, 200 University Ave. W, Waterloo, N2L 3G1, Canada
- <sup>2</sup> Canmet MATERIALS, Natural Resources Canada, 183 Longwood Rd S, Hamilton, ON, L8P 0A5, Canada
- \* Michael.benoit@uwaterloo.ca

Abstract: Increased adoption of recycled aluminum (Al) alloys in the automotive sector can provide several economic and environmental benefits through vehicle lightweighting, decreased fuel consumption, and reduction in greenhouse gas emissions. A major challenge in the adoption of secondary Al for a broader range of products is the accumulation of impurity elements, as increased scrap use can result in the compositional drift of alloy streams, leading to degraded mechanical and electrochemical properties. The objective of the current study is to demonstrate the use of rapid solidification processing (RSP) to increase the potential adoption of recycled Al through refinement of microstructural features and reduction of cracking. Cast ingots of an Al alloy 6061 (AA6061) were produced with iron (Fe) and zinc (Zn) additions in amounts ranging from 0 to 1 wt% to simulate recycling impurities. Thermodynamic simulations were used to predict the crack susceptibility of each alloy composition. Laser surface melting (LSM) trials were performed on plates cut from each ingot to generate rapidly solidified microstructures. The simulation predictions and microstructure results suggest that alloy impurity composition does influence the cracking behaviour observed in the laser melt pools, with both Fe and Zn additions having a mitigating effect on the observed cracking behaviour. The results suggest that the adoption of techniques such as additive manufacturing and laser welding could enable greater use of recycled Al alloys, advancing their use for automotive applications.

Keywords: AA6061, Cracking, Laser Surface Melting, Laser Welding, Recyclability

### 1. Introduction

Aluminum (Al) alloys find use in a wide range of applications across several industries and sectors owing to their good combination of properties, such as a high strength-to-weight ratio, good corrosion resistance, high thermal conductivity, etc. [1]. Recycled aluminum requires 95% less energy to produce compared to primary Al [2], reducing overall energy consumption and greenhouse gas emissions in its lifecycle. However, a major challenge to increasing the incorporation of secondary Al for use in commercial products is impurity tolerances, as increased levels of impurities can cause changes in the material's chemical and mechanical properties due to fundamental compositional changes, such as the formation of the deleterious  $\beta$ -AlFeSi phase and changes to intergranular corrosion resistance [3–5].

Iron (Fe) is a common impurity in Al and, at certain concentrations, can have an unwanted effect on the properties of the Al due to the depletion of elements, such as Si, to form less desirable intermetallic compounds (IMC) and impact corrosion resistance [1,6,7]. However, studies have found that increasing Fe content can also reduce susceptibility to hot tearing (solidification cracking) through the formation of beneficial IMC networks and grain refinement [1,7–11].

Zinc (Zn) can also be a prevalent impurity in recycled Al alloys through the mixed recycling of galvanized scrap with other Al parts [1]. Zinc has been shown to have minimal effects on the sequence in which precipitates form despite its high solubility in Al [7]. Furthermore, the inclusion of Zn has been shown to form  $MgZn_2$  precipitates in 6XXX series alloys processed under varying conditions, which have desirable mechanical properties [4,12]. However, Zn has been shown to negatively interact with the Q phase (AlMgSiCu) found at the grain boundaries, decreasing the intergranular corrosion resistance [1,4,5,7,12]

High cooling rates have often been used to tailor the solidification microstructure, selectively forming IMCs that contribute to the desired mechanical properties, refining the grain structure to reduce crack susceptibility, and mitigating harmful contributory impurities [10,13–16]. The objective of this study is to investigate the effect that fast-cooling rates, such as those characteristic of additive manufacturing (AM) processes, have on recycling-grade Al alloys through the use of laser surface melting (LSM).

#### 2. Materials and methods

## 2.1. Materials and sample preparation

Six compositions of cast AA6061 with Fe and Zn contents varying between 0 and 1 wt.% were investigated in the current study (Table 1). Details of the initial casting process used to fabricate the ingots are reported elsewhere [9]. Samples for LSM trials were prepared by machining 6.35 mm (1/4") thick slabs from the cast ingots. The surfaces of each slab were sandblasted to reduce their laser reflectivity.

Table 1. Al 6061 cast com	positions with varying	g Fe and Zn impuri	ty contents as measured by	spark OES	(in wt.%, bal. Al).

Alloy Designation	Fe	Zn	Si	Mg	Cu	Cr	Ti	Mn
6061	0.04	0.00	0.64	1.23	0.30	0.15	0.15	0.14
6061 + 0.25 Fe	0.24	0.00	0.60	1.16	0.31	0.14	0.17	0.14
6061 + 1 Fe	0.96	0.00	0.58	1.20	0.29	0.14	0.16	0.16
6061 + 1 Zn	0.05	0.98	0.62	1.24	0.31	0.15	0.14	0.14
6061 + 0.25 Fe + 1 Zn	0.24	0.99	0.60	1.21	0.30	0.15	0.15	0.14
6061 + 1 Fe + 1 Zn	0.95	1.01	0.59	1.20	0.30	0.15	0.15	0.15

# 2.2. Laser Surface Melting trials

Laser surface melting (LSM) was performed to create rapid solidification conditions characteristic of AM processes. Trials were performed using a Liburdi Automation LAWS 250 laser directed energy deposition (L-DED) machine, with a Nd: YAG laser (1064 nm, max power 1000 W, 2 mm spot size). Single melt tracks were produced for each alloy composition specified in Table 1 using eight parameter combinations. Laser powers of 750 and 950 W and scan speeds of 200, 300, 400, and 600 mm/min were used, resulting in linear energy densities ranging between 75 and 285 J/mm. Argon shielding gas at a flow rate of 10 L/min was used to protect the molten pool against oxidation. Each LSM track was a minimum of 45 mm in length and spaced 8 mm apart.

## 2.3. Microstructural characterization and analysis

Transverse cross sections were taken at 5 mm, 10 mm, and 20 mm from the start of each single track for each alloy composition and linear energy density condition, giving a total of 24 cross sections examined for each composition. Optical microscopy was performed on all sample cross sections using a Keyence VHX-6000 to identify the presence of cracks, pores, and intergranular liquid films. A VEGA3 TESCAN scanning electron microscopy (SEM) with back scattered electron (BSE) and energy dispersive spectroscopy (EDS) detectors was used for higher magnification imaging and chemical analysis.

### 3. Results and discussion

Optical micrographs of selected weld pools (black dashed lines) can be seen in Figure 1, in which several defects and microstructural features can be seen. The quantitative analysis of all defects from all process combinations for all alloy compositions considered is presented in Figure 1 f), in which the number of cross sections exhibiting specified defects is presented.

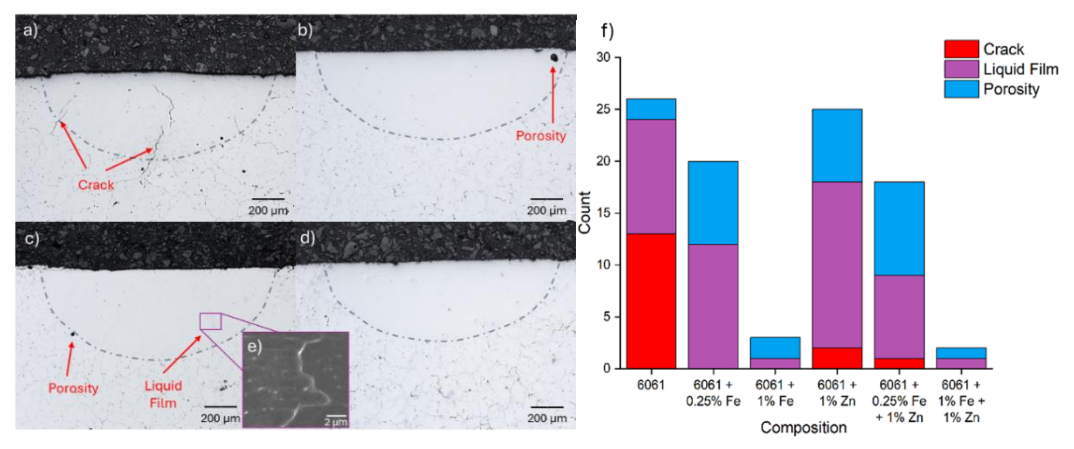


Figure 1. Optical microscopy of selected cross sections. a) 6061 950 W 600 mm/min b) 6061+1Fe 950 W 400 mm/min c) 6061+1Zn 950 W 200 mm/min d) 6061+1Fe+1Zn 750 W 400 mm/min e) Enlarged BSE SEM image of liquid film f) Quantitative

analysis of defect frequency vs. alloy composition. Count refers to the number of cross sections (24 max) in which specified microstructure features and defects were identified.

It can be seen from Figure 1 that the level of melt pool defects significantly decreased with increasing Fe content, with negligible defects noted for compositions with 1 wt.% Fe (1Fe). The addition of Zn to the base AA6061 composition also led to a decrease in cracking and an increase in liquid film formations. Liquid films can form at the end of solidification as the last liquid to freeze between solidifying grains or when backfilling an existing solidification crack. Gas porosity was observed across all compositions to varying degrees, with those containing 0.25 wt.% Fe having slightly higher occurrences. No clear trends in defect prevalence were observed with varying linear energy density, likely because all melt pools exhibited characteristics of conduction mode, resulting in minimal variation in melt pool shape.

Elemental mapping using SEM-EDS show the prevalence of Mg<sub>2</sub>Si phases in the base 6061 cast material and the formation of a crack propagating from the cast material into the remelt. The high levels of Si within the crack are attributed to the use of colloidal silica during metallography preparation (Figure 2a). The 1Fe + 1Zn alloy (Figure 2b) shows large eutectic particles enriched with Mg, Fe and Si, with refinement of these particles in the melt pool due to rapid cooling. Furthermore, no cracking or other defects were observed, and Zn is uniformly dispersed within the matrix.

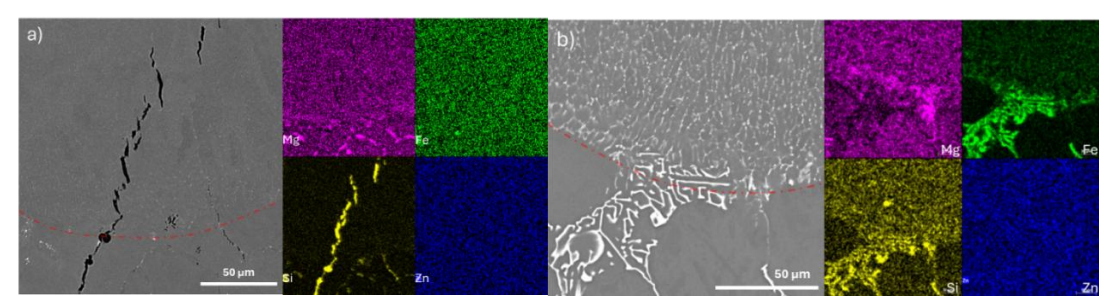


Figure 2. SEM images and EDS elemental maps of a) 6061 b) 6061 + 1 Fe +1 Zn. Red dashed line indicates the melt pool boundary.

To understand the composition-dependent crack susceptibility of AA6061 with Fe and Zn impurities, Kou's cracking index, which takes the maximum slope of the T vs.  $\sqrt{f_s}$  curve up to the coalescence point ( $f_{s,co}$ ) as shown in **Error! Reference source not found.**, was used [17]. In utilizing the criterion, a value of  $f_{s,co} = 0.97$  was selected [18]. ThermoCalc simulations using the Scheil-Gulliver model were performed for each composition listed in Table 1 to obtain the T vs  $f_{s,co}$  curves in Figure 3.

The index predicted a mitigating effect of Fe on cracking, which is in good agreement with the experimental results (Figure 1). Further examination using SEM-EDS analysis revealed a substantial increase in the volume fraction of highly refined particles containing Fe, Mg, and Si in the 6061+1Fe+1Zn melt pool compared to the baseline alloy. Previous studies have proposed that the formation of an interconnected network of fine  $\alpha$ -AlFeSi particles resists thermal stresses during cooling and mitigates cracking [8–10].

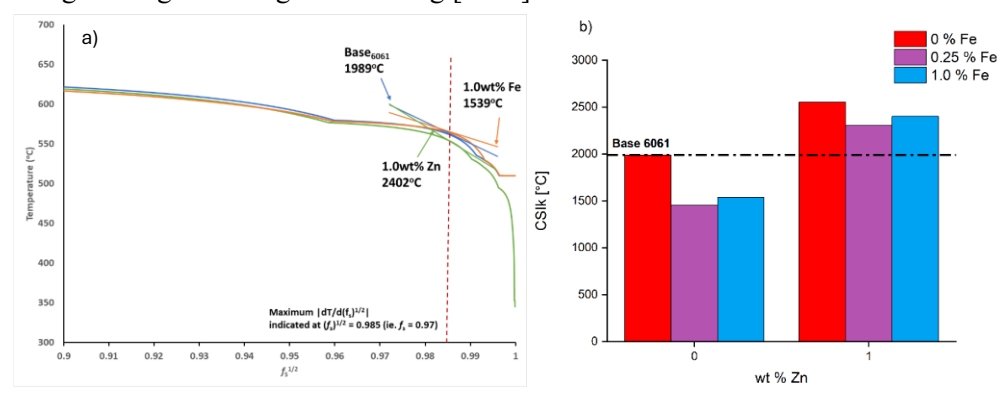


Figure 3. a) T- $\sqrt{f_S}$  curves for 6061, 6061 + 1 Fe, and 6061 + 1 Zn alloys with the max  $|dT/d\sqrt{f_S}|$  values at the coalescence point indicated. b) Comparison of CSI<sub>k</sub> values determined from T- $f_S^{1/2}$  plots, relative to base 6061 Al alloy (black dashed line)

The crack susceptibility predictions for Zn additions are not in agreement with experimental results, as the increase in liquid volume after dendrite coherency in samples containing 1 wt.% Zn resulted in the increase of liquid film formation rather than solidification cracks. However, this is represented as a steep temperature drop in the T vs.  $f_s$  curve, resulting in a large, predicted crack susceptibility. Moreover, it has been noted that Zn additions can alter the

solidification temperature and increase fluidity of the liquid phase, which would impact crack resistance [7]. In the SEM and EDS images seen in Figure 2b, Zn appears to be evenly distributed across both the cast material and the melt pool, due to its high solubility in aluminum and does not appear to be forming any deleterious IMCs. Additionally, Zn is known to form strengthening phases with magnesium that could also be contributing to the reduction of cracking in the alloys. Further investigation into the influence of Fe and Zn impurities on LSM of AA6061 is ongoing.

## 4. Conclusion

The effect of using rapid solidification processing to mitigate the potentially deleterious effects of Fe and Zn on AA6061 was investigated using laser surface melting trials. The following can be concluded from the results:

- Elevated Fe content led to reduced solidification defects compared to the baseline alloy, with increasing concentrations having a greater impact. The addition of 1 wt% Fe led to the elimination of nearly all defects related to solidification, notably cracking, regardless of other impurities.
- Elevated Zn content also reduced the quantity and severity of defects compared to base AA6061. Increased intergranular liquid film formation across compositions was noted.
- Non-equilibrium solidification simulations and a crack susceptibility index were able to correctly predict the mitigating effect of Fe on cracking but incorrectly predicted that elevated Zn levels would increase cracking.

# 5. Acknowledgments

The authors acknowledge the technical staff at CanmetMATERIALS for their assistance in casting the ingots used in this study and the technical staff at Liburdi Automation for their assistance in fabricating the laser melt tracks. The authors acknowledge the financial support of the NSERC Discovery Grant program (RGPIN-2021-02892).

#### 6. References

- [1] Davis JR, editor. Alloying: understanding the basics. Materials Park, OH: ASM International; 2001. 647 p.
- [2] Güley V, Ben Khalifa N, Tekkaya AE. Direct recycling of 1050 aluminum alloy scrap material mixed with 6060 aluminum alloy chips by hot extrusion. Int J Mater Form. 2010 Apr 1;3(1):853–6.
- [3] Modaresi R, Løvik AN, Müller DB. Component- and Alloy-Specific Modeling for Evaluating Aluminum Recycling Strategies for Vehicles. JOM. 2014;66(11):2262–71.
- [4] Guo MX, Du JQ, Zheng CH, Zhang JS, Zhuang LZ. Influence of Zn contents on precipitation and corrosion of Al-Mg-Si-Cu-Zn alloys for automotive applications. Journal of Alloys and Compounds. 2019 Mar;778:256–70.
- [5] Lutz A, Malet L, Dille J, De Almeida LH, Lapeire L, Verbeken K, et al. Effect of Zn on the grain boundary precipitates and resulting alkaline etching of recycled Al-Mg-Si-Cu alloys. Journal of Alloys and Compounds. 2019 Jul;794:435–42.
- [6] Nagaumi H, Suzuki S, Okane T, Umeda T. Effect of Iron Content on Hot Tearing of High-Strength Al-Mg-Si Alloy. Mater Trans. 2006;47(11):2821-7.
- [7] Mondolfo LF. Aluminium alloys: structure and properties. London; Butterworths,; 1976.
- [8] Sweet L, Easton MA, Taylor JA, Grandfield JF, Davidson CJ, Lu L, et al. Hot Tear Susceptibility of Al-Mg-Si-Fe Alloys with Varying Iron Contents. Metall Mater Trans A. 2013 Dec 1;44(12):5396–407.
- [9] Whitney MA, Jin H, Wells MA, Benoit MJ. Thermal analysis and characterization of cast 6061 aluminum alloy microstructures with elevated iron content. Thermochimica Acta. 2025 Apr;746:179951.
- [10] Benoit MJ, Whitney MA, Zhu SM, Zhang D, Field MR, Easton MA. The beneficial effect of minor iron additions on the crack susceptibility of rapidly solidified aluminum alloy 6060 toward additive manufacturing applications. Materials Characterization. 2023;205:113287.
- [11] Gremaud M, Carrard M, Kurz W. The microstructure of rapidly solidified Al-Fe alloys subjected to laser surface treatment. Acta Metallurgica et Materialia. 1990;38:2587–99.
- [12] Xu X, Zhu W, Yuan M, Liang C, Deng Y. The effect of Zn content on the microstructure and mechanical properties of the Al-mg-Si alloy. Materials Characterization. 2023 Apr;198:112714.
- [13] Li H ying, Zeng C ting, Han M sheng, Liu J jiao, Lu X chao. Time–temperature–property curves for quench sensitivity of 6063 aluminum alloy. Transactions of Nonferrous Metals Society of China. 2013 Jan;23(1):38–45.
- [14] Fabrizi A, Timelli G, Ferraro S, Bonollo F. Evolution of Fe-rich compounds in a secondary Al–Si–Cu alloy: influence of cooling rate: Paper presented at "XV International Conference on Electron Microscopy", 15–18 September 2014, Cracow, Poland. International Journal of Materials Research. 2015 Jul 4;106(7):719–24.
- [15] Qi X, Takata N, Suzuki A, Kobashi M, Kato M. Laser powder bed fusion of a near-eutectic Al–Fe binary alloy: Processing and microstructure. Additive Manufacturing. 2020 Oct;35:101308.
- [16] Ren W, Xu L, Qin C, Han Y, Zhao L, Hao K. Laser directed energy deposition additive manufacturing of Al7075 alloy: Process development, microstructure, and porosity. Journal of Materials Research and Technology. 2024 Nov;33:2093–100.
- [17] Kou S. A criterion for cracking during solidification. Acta Materialia. 2015 Apr;88:366-74.
- [18] Giraud E, Suery M, Adrien J, Maire E, Coret M. Hot tearing sensitivity of Al-Mg-Si alloys evaluated by x-ray microtomography after constrained solidification at high cooling rate. In: Hot Cracking Phenomena in Welds III. Heidelberg, Berlin: Springer; 2011. p. 87–99.